# Photoelectron spectra of dihalomethyl anions: Testing the limits of normal mode analysis

Kristen M. Vogelhuber,[1] Scott W. Wren,[1] Anne B. McCoy,[2]
Kent M. Ervin,[3] and W. Carl Lineberger[1,a)]

[1]*JILA and Department of Chemistry and Biochemistry, University of Colorado, 440 UCB, Boulder, Colorado 80309, USA*
[2]*Department of Chemistry, The Ohio State University, Columbus, Ohio 43210, USA*
[3]*Department of Chemistry and Chemical Physics Program, University of Nevada, Reno, Nevada 89557, USA*

We report the 364-nm negative ion photoelectron spectra of $CHX_2^-$ and $CDX_2^-$, where X = Cl, Br, and I. The pyramidal dihalomethyl anions undergo a large geometry change upon electron photodetachment to become nearly planar, resulting in multiple extended vibrational progressions in the photoelectron spectra. The normal mode analysis that successfully models photoelectron spectra when geometry changes are modest is unable to reproduce qualitatively the experimental data using physically reasonable parameters. Specifically, the harmonic normal mode analysis using Cartesian displacement coordinates results in much more C-H stretch excitation than is observed, leading to a simulated photoelectron spectrum that is much broader than that which is seen experimentally. A $(2 + 1)$-dimensional anharmonic coupled-mode analysis much better reproduces the observed vibrational structure. We obtain an estimate of the adiabatic electron affinity of each dihalomethyl radical studied. The electron affinity of $CHCl_2$ and $CDCl_2$ is 1.3(2) eV, of $CHBr_2$ and $CDBr_2$ is 1.9(2) eV, and of $CHI_2$ and $CDI_2$ is 1.9(2) eV. Analysis of the experimental spectra illustrates the limits of the conventional normal mode approach and shows the type of analysis required for substantial geometry changes when multiple modes are active upon photodetachment. © *2011 American Institute of Physics*. [doi:10.1063/1.3585606]

## I. INTRODUCTION

Dihalomethyl radicals $CHX_2$ (X = Cl, Br, and I) play significant roles in atmospheric chemistry, combustion, and organic synthesis. They are potential players in the depletion of atmospheric ozone. Partially halogenated chlorofluorocarbons—commonly used in refrigerants, fire suppressants, and pesticides—are oxidized in the troposphere to form, among other species, short-lived dihalomethyl radical products.[1–3] These radicals are then photolyzed by near-UV solar radiation to produce halogen atoms[1,4,5] that have been implicated in ozone loss and climate change.[6,7] Additionally, dihalomethyl radicals are by-products of the incineration of hazardous industrial waste, such as halogenated hydrocarbons, prompting research into the kinetic and thermodynamic properties of halomethyl radicals.[8] Halomethyl radicals are also of importance in several synthetic reactions, such as cyclopropanation of olefins and diiodomethylation of carbonyl compounds.[9–17]

Even though halomethyl radicals have been investigated by many groups over the past 40 years, much is still unknown about the dihalomethyl anions and their corresponding radicals. There have been a considerable number of matrix-isolation infrared spectroscopy studies of dihalomethyl radicals, specifically dichloromethyl radical, where several vibrational frequencies have been determined.[18–25] However, almost all of the observed modes are asymmetric vibrations, which are generally inactive in photoelectron spectroscopy. There has been only one spectroscopic observation of the dichloromethyl anion (FTIR Ar matrix isolation spectroscopy), from which two symmetric vibrational frequencies were determined.[26]

The thermochemistry of $CHCl_2$ and $CHBr_2$ radicals has also been studied by several groups.[27–29] The most recent and extensive experimental investigation was conducted by Nibbering *et al*.,[29] who performed bracketing experiments using FTICR mass spectrometry to study the occurrence or non-occurrence of electron transfer between a dihalomethyl radical anion and a neutral electron acceptor molecule with a known electron affinity (EA). In this way they determined the EAs of $CHCl_2$ and $CHBr_2$ to be 1.47(4) eV and 1.71(8) eV, respectively. One extensive theoretical study of halomethyl radicals and anions was performed by Li *et al*.[30] They published a computational review of the EAs, molecular structures, and thermochemistry of fluorine-, chlorine-, and bromine-substituted methyl radicals, comparing four independent density functional methods to known experimental values.

We study the dihalomethyl radicals using anion photoelectron spectroscopy. In anion photoelectron spectroscopy, a photon is used to detach an electron from a negative ion to produce a neutral radical. To a first approximation, the intensity of the neutral vibrational levels in a photoelectron spectrum is governed by the Franck–Condon overlap between the ground vibrational wavefunction of the anion with the wavefunctions of the various vibrational levels of the neutral. If

---

a)Author to whom correspondence should be addressed. Electronic mail: wcl@jila.colorado.edu.

there is little difference between the geometry of the anion and neutral, the best Franck–Condon overlap occurs between the ground vibrational wavefunction of the anion and the ground vibrational wavefunction of the neutral. This transition—the origin—appears as the most prominent peak in the spectrum, from which one can readily obtain the adiabatic EA. Also, the width of the photoelectron spectral envelope is minimal in the case of a small geometry change; the Franck–Condon region of the spectrum is confined to an area near the potential minimum of the neutral molecule, where vibrational modes can be well approximated as harmonic and uncoupled. For larger but still modest geometry changes between the two electronic states, long progressions of the vibrational modes will be observed and the Franck–Condon intensity for the origin peak may be much smaller than for the higher vibrational levels of the neutral corresponding to the vertical transition. Nevertheless, as long as the origin transition can be assigned, such spectra readily yield the quantitative spectroscopic quantities we hope to obtain from photoelectron spectroscopy.[31]

If a very large geometry change occurs between the anion and the neutral, however, spectral analysis becomes more difficult. When the Franck–Condon overlap for the origin transition is insignificant, only the transitions to high vibrational levels of the neutral are observed. At these higher vibrational levels, anharmonicity and mode coupling often become significant. In order to obtain vibrational frequencies and the EA, it is necessary to rely on theory and simulations for guidance. Even if vibrational progressions are well resolved, it may be impractical to extrapolate to the origin to find the EA.

In this work, we examine the photoelectron spectra of $CHCl_2^-$, $CHBr_2^-$, $CHI_2^-$, and their deuterated analogs. The spectra exhibit extended, partially resolved vibrational progressions that arise from the large geometry change that takes place when an electron is detached from the pyramidal anion, producing an essentially planar neutral radical. The observed vertical detachment energy (VDE), or the binding energy at the maximum of the vibrational progression, of each dihalomethyl radical is in good agreement with the calculated values,[30] providing us with confidence that theory can be used to accurately describe the electronic energies of these species. In contrast, a standard Franck–Condon analysis using normal modes in a Cartesian displacement coordinate system is inadequate for modeling these spectra. The partially resolved vibrational progressions in the simulated spectra do not agree with those observed, and deuteration yields changes in peak spacing opposite to what is predicted with simulation. Most important, the width of the envelope in the simulation is much greater than that which is observed. This failure of the harmonic normal mode simulation to reproduce the width of the measured spectral envelope is not normally observed.

These systems represent a very challenging case for Franck–Condon simulation and analysis, both because there is no detectable Franck–Condon intensity at the origin and because of the very different nature of the vibrational motions in the neutral compared with the anion. As we look to move beyond the standard normal mode treatment, we first consider the use of an internal coordinate system as the basis for the harmonic normal mode analysis, which can be expected to provide a better description of the geometry displacements than Cartesian coordinates but still does not adequately treat the anharmonicity of the vibrational potentials and coupling between modes. To treat those effects more accurately, we employ a multidimensional, anharmonic coupled-mode analysis for the key active modes. This investigation of dihalomethyl radicals explores the limits of conventional normal-mode analysis and illustrates the approaches required for transitions with a large geometry change and with multiple active, coupled, anharmonic modes.

## II. EXPERIMENTAL METHOD

The negative ion photoelectron spectrometer used in this experiment has been described in detail elsewhere.[31–33] The apparatus consists of four main sections: an ion source, a mass filter, an interaction region with crossed laser and ion beams, and an electrostatic electron kinetic energy analyzer. Negative ions are formed in a flowing afterglow ion source. A microwave discharge containing trace amounts of $O_2$ gas in He buffer gas ($\sim$0.4 Torr) generates atomic oxygen radical anion, $O^-$. The $O^-$ anion abstracts a H atom from methane that is added downstream, forming hydroxide anion ($OH^-$), which then deprotonates the appropriate dihalomethane precursor ($CH_2Cl_2$, $CH_2Br_2$, or $CH_2I_2$, Sigma-Aldrich) to generate dihalomethyl anions: $OH^- + CH_2X_2 \rightarrow CHX_2^- + H_2O$. The deuterated anion $CDX_2^-$ is produced by starting with perdeuterated dihalomethane $CD_2X_2$ ($CD_2Cl_2$, $CD_2Br_2$, and $CD_2I_2$, Sigma-Aldrich). Sufficient methane is added to ensure complete removal of $O^-$ before $CH_2X_2$ is introduced, guaranteeing that $CHX_2^-$ is produced exclusively, rather than having some $CX_2^-$ contaminant, which would be formed by the reaction $O^- + CH_2X_2 \rightarrow CX_2^- + H_2O$.[34] Collisions with He buffer gas cool the ions to $\sim$300 K. The flow tube can be further cooled with a liquid nitrogen jacket to obtain a "cold spectrum" of ions with temperatures near 150 K. The photoelectron spectra of $CHCl_2^-$ and $CDCl_2^-$ were collected at 150 K, while the spectra of $CHBr_2^-$, $CDBr_2^-$, $CHI_2^-$, and $CDI_2^-$ were collected at 300 K. Anions are extracted into a differentially pumped region and are accelerated to 735 V before entering a Wien velocity filter with a mass resolution of $m/\Delta m \sim 40$. The mass-selected ion beam (typically 100–500 pA) is decelerated to 35 V and focused into the interaction region. Here, the $\sim$0.5 W output from a single-mode continuous-wave argon ion laser operating at 364 nm (3.40814 eV) is built up to $\sim$50 W of circulating power in an optical buildup cavity located within the vacuum system. Photoelectrons ejected in the direction orthogonal to both the laser and ion beams enter a hemispherical energy analyzer. The photoelectron signal is recorded as a function of electron kinetic energy with a position-sensitive detector. The energy analyzer has a resolution of $\sim$12 meV under the conditions used for the present experiments.

The electron kinetic energy (eKE) can be converted to electron binding energy (eBE) through the relationship eBE $= h\nu - $ eKE. Absolute kinetic energies are calibrated[35] before each experiment using the well-known EA of O.[36]

Additionally, the electron energy scale is corrected for a slight linear compression (<1%) (Ref. [31]) using the photoelectron spectrum of W$^-$, which provides a number of known transitions spanning the photoelectron energy range.[37] After making these corrections and accounting for the resolution of the spectrometer and rotational peak profiles, absolute electron binding energies can be determined with an accuracy of 5 meV or better.[31]

A rotatable half-wave plate positioned outside the buildup cavity controls the polarization of the photodetachment radiation. When the angle between the laser polarization and the direction of the collected electrons is 54.7°, referred to as the magic angle, the photoelectron spectrum is independent of the anisotropy parameter of the ejected electrons.[38] Therefore, spectra collected at the magic angle directly reflect the total photodetachment cross section. All spectra shown here were collected with magic angle polarization.

## III. THEORETICAL METHODS

### A. Computational chemistry

In this work, we perform all electronic structure calculations using the GAUSSIAN 03 program package.[39] The geometry optimization and frequency calculations were performed with density functional theory using the B3LYP hybrid functional.[40,41] The calculations employ the 6–311++G(d,p) basis set for hydrogen, carbon, and chlorine,[42,43] and pseudopotentials for bromine and iodine that have been shown to work well for halogen-containing compounds.[44–46] Geometries were optimized, and harmonic vibrational frequencies and normal mode coordinates were calculated for the doublet anion and the singlet neutral states. The calculated equilibrium structures, relative energies, and frequencies of $CHCl_2$ and $CDCl_2$ are reported in Tables I and II; results of analogous calculations for $CHBr_2$ and $CHI_2$ are provided in supplementary material (Tables S1–S4).[47] In addition to the non-planar minimum energy structures of the anionic and neutral $CHCl_2$ and $CDCl_2$, we also consider the low-lying saddle point on the neutral surface in which all four atoms are coplanar. This structure is calculated to be only 162 cm$^{-1}$ above the minimum on this surface at the present level of theory. This energy is smaller than half the harmonic frequency of the CH (CD) pyramidal bend, leading us to ex-

pect that when zero-point motion is considered the ground state wavefunction will be delocalized and will have significant amplitude at the transition state geometry. The inversion barriers for $CHBr_2$ and $CHI_2$ (160 cm$^{-1}$ and 1 cm$^{-1}$, respectively) are likewise smaller than half the harmonic frequency of the CH (CD) pyramidal bend in both of these systems (Table III).

### B. Franck–Condon analysis using Cartesian coordinates

We typically use a Franck–Condon analysis of the vibrational structure in photoelectron spectra to obtain frequencies and equilibrium geometries of the neutral species and to identify the origin transition. This method is used to simulate the photoelectron spectrum of the furanide anion ($C_4H_3O^-$), which we will use as a prototype for analysis of photoelectron spectra. The intensity of a vibronic transition $I_{FC}$ is proportional to the square of the Franck–Condon overlap integral,

$$I_{FC} = \left[ \int \psi_{\nu'}(\mathbf{Q}')\psi_{\nu''}(\mathbf{Q}'')d\mathbf{Q}' \right]^2, \quad (1)$$

where $\psi_{\nu'}(\mathbf{Q}')$ is the full, multidimensional vibrational wavefunction of the neutral in quantum state $\nu'$ as a function of the normal coordinates of the neutral $\mathbf{Q}'$, and $\psi_{\nu''}(\mathbf{Q}'')$ is the corresponding vibrational wavefunction of the anion in terms of its normal coordinates $\mathbf{Q}''$. The normal modes are treated as uncoupled and harmonic.[48]

It is necessary to express the wavefunctions of both the anion and the neutral states in terms of the same set of normal coordinates in order to calculate the Franck–Condon overlap integral. The Duschinsky transformation[49] is applied to express the normal mode coordinates of the neutral in the basis set of the normal mode coordinates of the anion. The transformation is given by

$$\mathbf{Q}'' = \mathbf{J}''\mathbf{Q}' + \mathbf{K}''. \quad (2)$$

Here, $\mathbf{K}''$ is the vector that describes the difference in the nuclear equilibrium positions between the anion and neutral in terms of the normal coordinates of the anion. The Duschinsky rotation matrix $\mathbf{J}''$ accounts for mixing of normal modes resulting from the discrepancy between the normal mode

TABLE I. Calculated, unscaled harmonic vibrational frequencies of $CHCl_2^-$, $CHCl_2$, $CDCl_2^-$, and $CDCl_2$ (B3LYP/6–311++G(d,p)), given in units of cm$^{-1}$. Experimental frequencies (where available) are listed in italics.

| | | | CHCl$_2$ | | | CDCl$_2$ | |
|---|---|---|---|---|---|---|---|
| | Vibrational mode | CHCl$_2^-$ | Pyramidal, C$_s$ | Planar, C$_{2v}$ | CDCl$_2^-$ | Pyramidal, C$_s$ | Planar, C$_{2v}$ |
| A$'$ | HCCl *sym bend* | 212.5 | 304.4 | 310.4 (A$_1$) | 211.5 | 302.4 | 308.5 (A$_1$) |
| | ClCCl *sym str* | 497.2, *532*[a] | 748.1, *845*[b] | 741.0 (A$_1$) | 494.0 | 715.1, *814*[b] | 720.2 (A$_1$) |
| | CH *pyram bend* | 1029.4 | 469.5 | 352.3i (B$_1$) | 768.3 | 384.6 | 285.6i (B$_1$) |
| | CH *stretch* | 2917.8, *2764*[a] | 3216.7 | 3255.8 (A$_1$) | 2146.4 | 2368.8 | 2398.6 (A$_1$) |
| A$''$ | ClCCl *asym str* | 399.8 | 865.6, *902*[c] | 897.5 (B$_2$) | 396.8 | 805.1, *814*[c] | 818.0 (B$_2$) |
| | CH *asym wag* | 1172.2 | 1249.7, *1226*[c] | 1242.5 (B$_2$) | 846.5 | 965.0, *974*[c] | 979.3 (B$_2$) |

[a]Experiment, Ar matrix: Richter *et al.*, 1997 (Ref. [26]).
[b]Experiment, REMPI: Long and Hudgens, 1987 (Ref. [67]).
[c]Experiment, Ar matrix: Carver and Andrews, 1969 (Refs. [18] and [19]).

TABLE II. Calculated equilibrium structures of $CHCl_2^-$ ($CDCl_2^-$) and $CHCl_2$ ($CDCl_2$) obtained using B3LYP/6–311++G(d,p). Bond lengths are in units of Å and angles are in units of degrees. The geometry change upon photodetachment is defined as the difference in the values of the internal coordinates for the anion and the radical.

| Internal coordinate | $CHCl_2^-$ ($CDCl_2^-$) | Geometry change, neutral–anion | |
| --- | --- | --- | --- |
| | | Pyramidal, $C_s$ | Planar, $C_{2v}$ |
| $r_{CH}$ | 1.105 | −0.025 | −0.028 |
| $r_{CCl}$ | 1.958 | −0.239 | −0.249 |
| $\theta_{HCCl}$ | 96.0 | 20.7 | 23.6 |
| $\theta_{ClCCl}$ | 105.2 | 14.1 | 15.6 |
| $\tau_{ClCHCl'}$ | 106.0 | 44.2 | 74.0 |

coordinates of the anion and neutral.[48] By basing the analysis on harmonic wave functions expressed in terms of the normal coordinates, the above approach will be exact in the limit that the Hamiltonian is quadratic in these coordinates and their conjugate momentum.

The Franck–Condon profiles of the photoelectron spectra are simulated using the PESCAL program.[50] Since none of the frequencies of the allowed vibrational modes for the dihalomethyl species are known experimentally, the simulations use theoretical geometries, normal mode vectors, and vibrational frequencies of the anion and neutral states calculated using the GAUSSIAN 03 software package.[39] The normal mode eigenvectors ($\mathbf{Q'}$, $\mathbf{Q''}$) are expressed in terms of mass-weighted Cartesian atomic displacement coordinates, and the Duschinsky rotation $\mathbf{J''}$ matrix and displacement vector $\mathbf{K''}$ are determined using Eq. (2). The Franck–Condon intensities for all six modes as well as their combination bands and hot bands (at 150 K for $CHCl_2^-$ and $CDCl_2^-$; and at 300 K for $CHBr_2^-$, $CDBr_2^-$, $CHI_2^-$, and $CDI_2^-$) are computed in the harmonic oscillator approximation including Duschinsky rotation using the Sharp-Rosenstock-Chen method.[51–53] The normal mode simulations of $CHCl_2^-$ and $CDCl_2^-$ are computed with an EA of 1.3 eV. The individual vibronic peak contours are approximated as a Gaussian function with a 12 meV FWHM, consistent with instrumental resolution.

## C. Franck–Condon analysis using internal coordinates

The normal mode analysis using orthogonal Cartesian displacement coordinates is easily implemented computationally for molecules of arbitrary size and connectivity, and therefore has become the conventional method.[54] These normal modes are, to the lowest order, identical to the normal modes in internal coordinates (bond lengths and angles) for infinitesimal displacements, but become less reasonable for large geometry changes. The older **GF**-matrix techniques using internal coordinates as described by Wilson *et al.*,[55] as well as more recent formulations,[56] require calculations specific to each system. It has been shown that using curvilinear internal coordinates in the normal mode analysis is more accurate for Franck–Condon simulations of systems with large geometry changes.[57,58] As the internal coordinates more naturally represent the vibrational potential energy surfaces, they are less likely to induce artificial couplings between modes in the mode displacements, **K**, and the Duschinsky rotation matrix.

We implement the harmonic normal mode analysis using the internal coordinates represented by the three bond stretches (CH, CX, and CX′) and three bond angles (HCX, HCX′, and XCX). We start from the force constant matrix in internal coordinates from GAUSSIAN 03,[39] and derive the Wilson **B**-, **G**-, and **F**-matrices analytically.[55] The Wilson **GF** method[55] is used to compute the normal modes and frequencies, which are verified to match those calculated using the Cartesian coordinate system. These analytical calculations were implemented using MATHEMATICA (Wolfram Research Inc.). The resulting normal mode vectors in the internal displacement coordinate basis are then used to calculate via Eq. (2) the corresponding **K″** displacements and Duschinsky **J″** rotation matrix, which is now a non-orthogonal transformation.[57,58] A modified version of PESCAL (Ref. 50) is used to obtain the Franck–Condon factors (FCFs), again in the harmonic oscillator approximation including Duschinsky rotation using the Sharp-Rosenstock-Chen method.[51–53] The spectra of $CHCl_2^-$ and $CDCl_2^-$ are simulated at 150 K, while the spectra of $CHBr_2^-$, $CDBr_2^-$, $CHI_2^-$, and $CDI_2^-$ are simulated at 300 K. As before, the simulations of $CHCl_2^-$ and $CDCl_2^-$ are computed with an EA of 1.3 eV, and the

TABLE III. The experimental and calculated (B3LYP/6–311++G(d,p)) EA, VDE, and peak spacing near the VDE for each of the dihalomethyl radicals. Basis sets and pseudopotentials for Br and I were developed by Stoll *et al.* (Refs. 44–46).

| | | $CHCl_2$ | $CDCl_2$ | $CHBr_2$ | $CDBr_2$ | $CHI_2$ | $CDI_2$ |
| --- | --- | --- | --- | --- | --- | --- | --- |
| EA (eV) | Experiment | 1.3(2)[a] | 1.3(2)[a] | 1.9(2)[a] | 1.9(2)[a] | 1.9(2)[a] | 1.9(2)[a] |
| | | 1.47(4)[b] | | 1.71(8)[b] | | | |
| | Calculation | 1.430 | 1.433 | 1.744 | 1.747 | 1.820 | 1.826 |
| VDE (eV) | Experiment | 2.6487 | 2.6815 | 3.0181 | 3.0171 | 2.8287 | 2.9057 |
| | Calculation | 2.8621 | 2.8630 | 2.8829 | 2.8836 | 2.8271 | 2.8271 |
| Peak spacing near VDE (cm$^{-1}$) | Experiment | 190(50) | 231(6) | 520(30) | 170(40) | 440(40) | 380(60) |
| | Normal mode | 240(10) | 361(9) | 205(1) | 303(9) | 540(10) | 511(7) |
| | (2 + 1)-D | 150(20) | 240(10) | ... | ... | ... | ... |
| Inversion barrier (cm$^{-1}$) | Calculation | 162 | 162 | 160 | 160 | 1 | 1 |

[a]Estimates of EA were obtained by subtracting the calculated difference in energy between the VDE and the EA (VDE$_{calc}$ − EA$_{calc}$) from the experimentally measured VDE using Eq. (8).
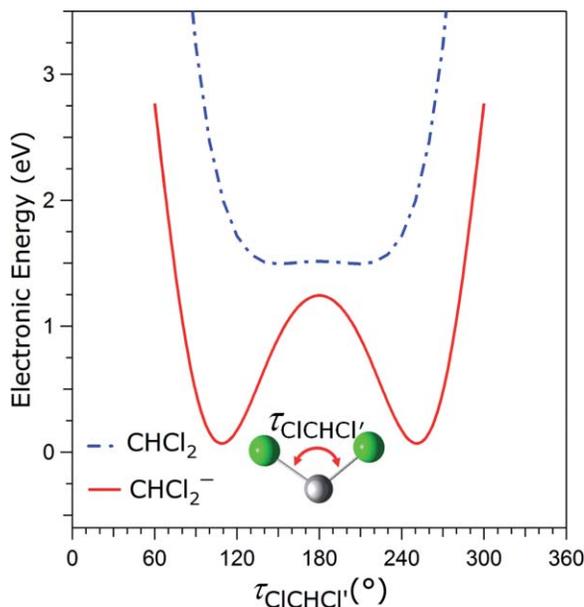[b]Experiment, Fourier transform ion cyclotron resonance mass spectrometry (Ref. 29).

FIG. 1. $CHCl_2$ (dashed blue) and $CHCl_2^-$ (red) potential energy curves as a function of the out-of-plane angle ($\tau_{ClCHCl'}$).

individual vibronic transitions are convoluted over the instrumental resolution function for comparison with experiment.

## D. (2 + 1)-dimensional anharmonic coupled-mode analysis

Although the harmonic normal mode analysis using the internal coordinate system is an improvement over the Cartesian coordinates for systems with large geometry changes, it does not address either the anharmonicity of the vibrational potentials or coupling between vibrational modes within one electronic state. To address these issues, we take a multidimensional anharmonic coupled-mode approach instead. For this challenging system, we explicitly couple the two bend modes and convolute the resulting spectrum with the spectrum obtained from a one-dimensional treatment of the ClCCl stretch in an overall (2 + 1)-dimensional coupled mode analysis.

First, we must choose a reduced set of vibrations that is appropriate for the dihalomethyl system. Based on calculated geometry changes between the minimum energy structure of the anion and neutral species listed in Table II, we anticipate that the three most important modes contributing to the photoelectron spectrum will be the ClCCl symmetric stretch, the HCCl (DCCl) symmetric bend, and, most importantly, the out-of-plane distortion of $CHCl_2$ ($CDCl_2$). We generate a calculated photoelectron spectrum in two parts. The first focuses on the ClCCl symmetric stretch contribution, while the second involves the HCCl symmetric bend and out-of-plane bending modes. We explicitly couple the two bending modes because we calculate a large change in the HCCl angle as the out-of-plane bend is distorted from the planar structure. This is illustrated in Fig. 1, in which the potential energy curves for $CHCl_2$ (dashed blue) and $CHCl_2^-$ (red) are plotted as a function of the out-of-plane distortion, defined as the ClCHCl' improper torsion angle $\tau_{ClCHCl'}$, minimizing the energy with respect to the displacements of the remaining



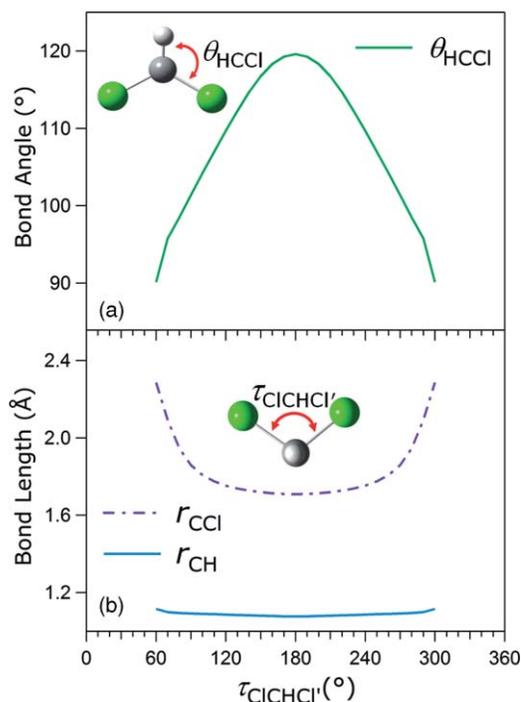FIG. 2. Change in the $CHCl_2$ internal coordinates $\theta_{HCCl}$ (green), $r_{CCl}$ (dashed purple), and $r_{CH}$ (blue) as the out-of-plane angle $\tau_{ClCHCl'}$ is varied.

coordinates.[56] This improper torsion is defined as the angle between the plane containing the carbon, hydrogen, and one of the chlorine atoms and the plane that contains the carbon, hydrogen, and the other chlorine atom, as illustrated in the inset in Fig. 1. The minimum energy structure of the anion corresponds to a value of $\tau_{ClCHCl'}$ of 106°. Based on the plots of the other three internal coordinates along this potential cut (Fig. 2), we find that there are large differences in the values of the HCCl angles (green), and, to a lesser extent, the CCl distance (dashed purple) as $\tau_{ClCHCl'}$ is decreased from 180° to 106°. The changes in the CH bond length (blue) are much smaller. As the equilibrium CH bond length is effectively independent of $\tau_{ClCHCl'}$ and its frequency is significantly higher than the other symmetry-allowed vibrational modes, we expect that the CH stretching vibrational motion will not contribute to the photoelectron spectrum or couple strongly to active modes. This expectation was further confirmed by reduced dimensional studies involving this mode and the out-of-plane distortion.

Once the active modes have been selected, we evaluate cuts through the six-dimensional potential energy surface as functions of these coordinates. For the two-dimensional cut along the two bending coordinates, we allow the remaining two symmetric coordinates to vary in order to minimize the electronic energies. This cut is evaluated over a range from $\theta_{HCCl} = 60°$ to 140° (in increments of 10°, with both HCCl angles kept equal), and from $\tau_{ClCHCl'} = 60°$ to 300° (in increments of 10°). A bicubic spline interpolation scheme was used to interpolate the potential between these points. The cut along the ClCCl stretch coordinate was evaluated over a range of $r_{CCl}$ from 1.2 Å to 2.7 Å in increments of 0.05 Å, with the two CCl distances constrained to be equal. For this cut the other coordinates are constrained to their equilibrium values

on the anion surface. Two-dimensional cuts through the anion and neutral potentials are provided in supplementary material (Fig. S1).[47]

Using these surfaces, we evaluate the vibrational energies and wavefunctions for the two subsystems. Just as the potentials are evaluated independently, two separate calculations are performed to obtain these quantities. To examine the ClCCl symmetric stretch, we define the coordinate $s$ as the symmetric combination of the two CCl distances $r_{CCl}$, which are constrained by symmetry to be equal. Thus, for the ClCCl stretch, we define $s = \sqrt{2}r_{CCl}$. As such,

$$H = -\frac{\hbar^2}{2}\left[\frac{1}{m_{Cl}} + \frac{\left(1 + \cos\theta_{CHCl,e}^{(\alpha)}\right)}{m_C}\right]\frac{\partial^2}{\partial s^2} + V^{(\alpha)}(s),$$
(3)

where $\alpha$ can represent the potential for either the anion or neutral system. As there is no dependence of the kinetic energy on the mass of the hydrogen atom, the energies and wavefunctions will be identical for CHCl$_2$ and CDCl$_2$. The Schrödinger equation is evaluated in a discrete variable representation (sinc-DVR), as described by Colbert and Miller.[59] Specifically, 500 DVR points are used with $r_{CCl} = s/\sqrt{2}$ ranging from 1 to 2.5 Å.

In a second calculation, we evaluate the energies and wavefunctions for the two-dimensional bend problem, where the two bend coordinates are denoted $\tau_{ClCHCl'}$ for the out-of-plane distortion and $\theta_s$ for the symmetric HCCl bend. We define the HCCl symmetric bend as the symmetric combination of the two equivalent $\theta_{HCCl}$. Thus, $\theta_s = \sqrt{2}\theta_{HCCl}$. Here,

$$H = \frac{1}{2}\big[p_\tau G_{\tau,\tau} p_\tau + p_\tau G_{\tau,\theta} p_\theta + p_\theta G_{\tau,\theta} p_\tau + p_\theta G_{\theta,\theta} p_\theta$$
$$+ V_{2d}^{(\alpha)}(\tau,\theta_s) + V'(\tau,\theta_s)\big].$$
(4)

For this expression, the values of the **G**-matrix elements and $V'$ are obtained from the tabulation of Frederick and Woywod.[56] The **G**-matrix elements depend on the two bend coordinates. The matrix representation of multiplicative operators, including the **G**-matrix elements, is diagonal in the DVR, whereas the momentum operators are not. As a result, in a DVR, the matrix elements are of the form

$$\langle n_\tau, n_\theta | p_i p_j G_{i,j}(\tau,\theta) | m_\tau m_\theta \rangle$$
$$= \langle n_\tau, n_\theta | p_i p_j | m_\tau m_\theta \rangle G_{i,j}(\tau_{m_\tau}, \theta_{m_\theta})$$
(5)

and

$$\langle n_\tau, n_\theta | G_{i,j}(\tau,\theta) p_i p_j | m_\tau m_\theta \rangle$$
$$= \langle n_\tau, n_\theta | p_i p_j | m_\tau m_\theta \rangle G_{i,j}(\tau_{n_\tau}, \theta_{n_\theta}).$$
(6)

Since analytical expressions for $\langle n_\tau, n_\theta | p_i p_j | m_\tau, m_\theta \rangle$ in a sinc-DVR are known,[59–61] expressing the terms in the kinetic energy operator in this form greatly simplifies the calculation. To ensure that the kinetic energy operator is Hermitian, we rewrite the kinetic terms in Eq. (4) as[60]

$$p_i G_{ij}(q_i,q_j)p_j = \frac{1}{2}\bigg[p_i p_j G_{i,j}(q_i,q_j)$$
$$+ G_{i,j}(q_i,q_j)p_i p_j - \hbar^2\frac{\partial^2 G_{ij}}{\partial q_i \partial q_j}\bigg].$$
(7)

Finally, the matrix elements of $p_i$ in a sinc-DVR have been worked out by Luckhaus.[60] In this work, we use an infinite grid limit of this expression, reported in Gardeinier *et al.*[61] For the calculations reported here, we use 50 evenly spaced grid points in each dimension and a range that spans the range of electronic energies.

Within the Franck–Condon approximation, the calculated photoelectron spectrum is obtained by first evaluating the squared overlaps of the vibrational states of the anion with energies less than 1000 cm$^{-1}$ above the ground vibrational state with all of the calculated states on the neutral surface for each of the two potential cuts described above. To account for the increase in the frequency of the ClCCl stretch between the minimum energy geometry on the neutral surface to the region of the potential that is sampled in the spectrum (e.g., the minimum energy geometry of the anion), the anharmonic energies of the ClCCl stretch are multiplied by 1.08. This is the ratio of the frequency of this mode when $\tau_{ClCHCl'}$ and $\theta_s$ are constrained to their values in the vertical and equilibrium geometries on the neutral surface. We combine the two stick spectra, weighting the product of the overlaps by a Boltzmann factor of $\exp[-(E_{stretch} + E_{bend})/k_bT]$, where the energies are obtained from the one- and two-dimensional calculations and $T = 150$ K. We then convolute the resulting spectrum with Gaussian functions with FWHM of 12 meV. The calculated spectra were shifted so that the adiabatic EA is in agreement with the experimental value of 1.3 eV.

## IV. RESULTS

### A. Experimental spectra and qualitative analysis

The anion photoelectron spectra of CHCl$_2^-$, CHBr$_2^-$, CHI$_2^-$, and their deuterated analogs are shown in Fig. 3. All of the spectra display extensive vibrational progressions resulting from the large geometry change that takes place upon photodetachment. The most prominent features in the spectra result from Franck–Condon overlap with high vibrational levels of the neutral. The calculated EA and calculated VDE of each dihalomethyl radical is marked with a labeled arrow in Fig. 3. The calculated EAs are consistent with previous experimental EA determinations of CHCl$_2$ and CHBr$_2$ (Table III).[29] In each case, the origin is calculated to lie at least 1 eV below the VDE—approximately the eBE at the peak of the vibronic band—in a region of negligible signal because of poor Franck–Condon overlap. However, the calculated VDEs, computed by subtracting the energy of the anion from the energy of the neutral at the equilibrium geometry of the anion, agree reasonably well with the measured VDEs of the dihalomethyl anions, as shown in Fig. 3 and listed in Table III. From the Franck–Condon simulations, the origin transition is calculated to have $\sim 10^{-5}$ the intensity of the peak at the VDE. Thus, the origin will not be experimentally observable. The calculation of the difference in energy between the VDE and the EA should be fairly accurate in the case of rigid anions such as the dihalomethyl anions, so we can use the following equation to obtain an estimate of the EA:

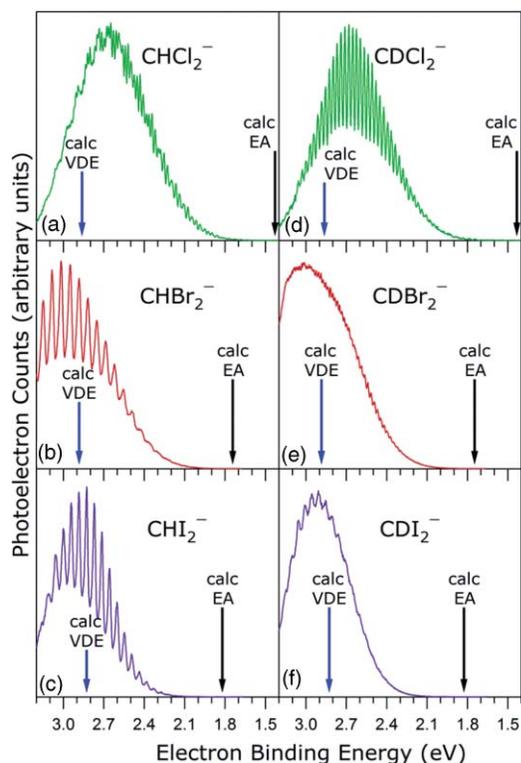$$EA_{est} = VDE_{exp} - [VDE_{calc} - EA_{calc}],$$
(8)

FIG. 3. Experimental spectra of the dihalomethyl anions (a) $CHCl_2^-$, (b) $CHBr_2^-$, (c) $CHI_2^-$, (d) $CDCl_2^-$, (e) $CDBr_2^-$, and (f) $CDI_2^-$. The calculated (B3LYP/6–311++G(d,p)) adiabatic electron affinity (EA) and vertical detachment energy (VDE) for each dihalomethyl radical is marked with a labeled arrow.

where

$$VDE_{calc} = E(\text{neutral at anion eqm geometry})$$
$$-E(\text{anion at anion eqm geometry}) \qquad (9)$$

and

$$EA_{calc} = E(\text{neutral at neutral eqm geometry})$$
$$-E(\text{anion at anion eqm geometry}). \qquad (10)$$

In this way, an estimate of the EA of each dihalomethyl radical studied is determined using the experimental VDE and the calculated difference between the energy of the anion and the energy of the neutral at the anion equilibrium geometry. These results are summarized in Table III. Our estimates are consistent with the previous EA determinations of $CHCl_2$ and $CHBr_2$.[29] The estimated EA of each dihalomethyl radical obtained from Eq. (8) is used as the EA for the simulations and calculations of that radical.

There are several indications that the structure in the spectra does not result from a single vibrational progression and instead arises from multiple active vibrational modes with several vibronic transitions lying under each peak. First, the spacing between the peaks in the spectrum of $CDCl_2^-$ does not correspond to the calculated frequency of any of the symmetric vibrational modes. Second, isotopic substitution has an unexpected effect on the spectrum of $CHCl_2^-$. The spectrum generally becomes more congested upon deuteration, as seen

in the spectra of $CHBr_2^-$ and, to a lesser extent, of $CHI_2^-$. However, the spectrum of $CDCl_2^-$ has more resolved structure than that of $CHCl_2^-$, implying that the observed structure is due to accidental resonance among two or more vibrational modes, rather than to a single vibrational progression. Also, the peak widths near the VDE are at least 20 meV, significantly greater than our experimental resolution of about 12 meV. Furthermore, the modulation depth of the peaks and the peak spacings change across the progression, a result of anharmonicity causing the vibronic transitions to move in and out of the resonance.

Although the spectra show that multiple active vibrational modes give rise to the observed structure, the similarity of the $CHBr_2^-$ and $CHI_2^-$ spectra suggests that the out-of-plane bend is active and that the spacing of the peaks roughly corresponds to the frequency of this motion in the neutral species. In $CHBr_2$, the average peak spacing is 520(30) $cm^{-1}$, and in $CHI_2$ it is 440(40) $cm^{-1}$ near the VDE (Table III). All of these observations are summarized in Table III.

As a large geometry change takes place when an electron is removed from a dihalomethyl anion to generate the floppy radical, further quantitative analysis of the spectra is difficult. We now turn to calculations and simulations to elucidate the spectra. To illustrate the challenges involved in analyzing the photoelectron spectra of molecules that undergo large geometry changes upon photodetachment, we examine in detail the agreement between experiment and theory for $CHCl_2^-$ and $CDCl_2^-$.

## B. Franck–Condon simulation using normal mode analysis in Cartesian coordinates

We initially simulate the spectra of $CHCl_2^-$ and $CDCl_2^-$ with Franck–Condon analysis using the methods outlined in Sec. III B, the harmonic oscillator approximation with normal modes calculated in the mass-weighted Cartesian displacement coordinate system. The Duschinsky rotation between the normal mode vectors of the anion and neutral is fully treated. This standard approach very accurately simulates electronic spectra that involve relatively small displacements of equilibrium geometries of the neutral relative to the anion;[57,62–64] in those cases, the most prominent features in the spectra arise from overlap between the lowest vibrational levels of each state, where the vibrations are well described as decoupled harmonic oscillators. Furthermore, if the equilibrium geometries and bonding of the two states are very similar, the character of their normal modes is essentially the same and the Duschinsky rotation effects may be minor.

The furanide anion illustrates such a case. The Franck–Condon simulation of the photoelectron spectrum of the furanide anion,[64] shown in Fig. 4(a), quantitatively reproduces the measured spectral envelope and vibrational structure. In the case of the furanide anion, the relatively rigid ring structure constrains the molecule to a modest geometry change upon photodetachment. Thus, we observe a prominent origin peak from which we directly obtain the EA of the furanyl radical. Despite the fact that furanyl has 13 allowed symmetric vibrational modes—compared to four symmetric modes in the

dihalomethyl anions—the furanide spectrum is dominated by signatures from only three of these. As one would intuitively expect, the most active vibrations are ring deformations localized around the radical center, whence the excess electron is detached. The excellent agreement between the normal-mode based simulation and experiment enables assignment of the spectral features, allowing unequivocal determination of the EA and identification of the frequencies of the most active vibrational modes. Furthermore, deviations from the predicted photoelectron spectrum occur at higher vibrational levels of the furanyl radical and can generally be corrected by simply accounting for frequency shifts of the transitions due to anharmonicity. Although the furanide anion is much larger and has many more allowed vibrational modes than the dihalomethyl anions, the fact that it undergoes a relatively small geometry change upon photodetachment means that its photoelectron spectrum is relatively straightforward to interpret, and from it we can determine a great deal of information about the furanyl radical. The Franck–Condon simulation—with vibrational parameters extracted from Gaussian output files and using the PESCAL program[50] to generate FCFs and convolute over the instrumental resolution and rotational contours—is largely an automated process in such a case.

As the normal mode method for modeling photoelectron spectra has proven so powerful in the past, we first employ a Franck–Condon analysis using normal modes based in Cartesian coordinates to interpret the photoelectron spectra of the dihalomethyl anions. In Fig. 4(b), we compare the experimental spectrum of $CDCl_2^-$ to its Franck–Condon simulation using the Cartesian coordinate system. In stark contrast to the excellent agreement between simulation and experiment displayed in the furanide case [Fig. 4(a)], the simulation in panel (b) utterly fails to reproduce the spectral envelope of the observed $CDCl_2^-$ spectrum. Similarly broad progressions are calculated for the other dihalomethyl anions. Examination of the Franck–Condon intensities shows that the reason for the disparity in the width of the spectral envelope is due to false strong activity of the CH (CD) stretch vibrational mode. This activity is inconsistent with the calculated geometries (Table II), which show only a relatively small change in the CH bond length between the anion and neutral states (an order of magnitude smaller than the CCl bond length change). Evidently, the only way the rectilinear Cartesian coordinates can reproduce the large geometry change is by inducing a spurious displacement in the CH stretch normal mode, in combination with other modes. Thus, there is a non-physical activation of the CH stretch associated with the pyramidal bend. Similar mode mixing has been observed for other molecules undergoing large geometry changes upon photodetachment,[55,57,58,65,66] where a large geometry displacement in one Cartesian coordinate is partially projected onto the others, resulting in the appearance of vibrational progressions in the computed spectrum that are not experimentally observed. For a molecule undergoing a substantial geometry change upon photodetachment, this effect is exacerbated when the Cartesian coordinate representation is used, resulting in the dramatically extended vibrational progression in Fig. 4(b).[47] Such poor agreement does not enable quantitative analysis of the photoelectron
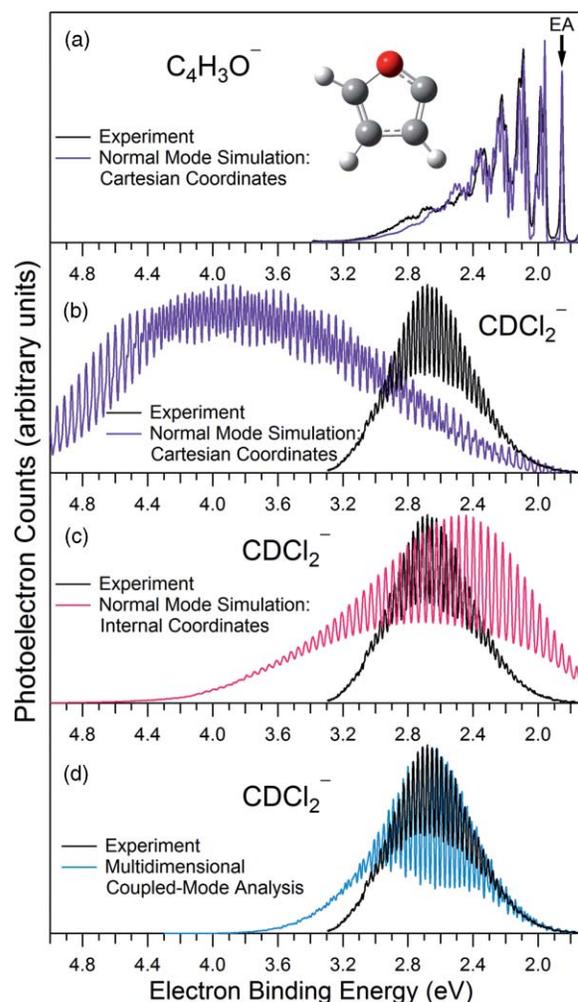


FIG. 4. Comparison between theory and experiment for two systems: (a) the furanide anion, $C_4H_3O^-$, and (b)–(d) $CDCl_2^-$. (a) The photoelectron spectrum (300 K, $\theta = 0°$) of furanide is compared to its ground state simulation using normal mode analysis in Cartesian coordinates. This is in sharp contrast to (b) the agreement between the photoelectron spectrum of $CDCl_2^-$ (150 K) and its simulation using normal mode analysis in Cartesian coordinates, which fails to reproduce the width of the spectral envelope. (c) Improvement in the agreement between experiment and the normal mode simulation is achieved by switching to an internal coordinate representation. (d) The width of the calculated spectral envelope is further reduced by using $(2 + 1)$-dimensional anharmonic coupled-mode analysis. All $CDCl_2^-$ calculated and simulated spectra were calculated at 150 K and were shifted to match the experimental EA of 1.3 eV.

spectra of the dihalomethyl anions, so we must take a more sophisticated approach to analyzing these spectra.

## C. Franck–Condon analysis using internal coordinates

For a better approximation of the vibrational displacement between the anion and neutral in the $CHX_2$ system, we next carry out the normal mode analysis using internal displacement coordinates as described in Sec. III C. The experimental spectrum of $CDCl_2^-$ is compared to its Franck–Condon simulation using normal modes in the internal coordinate representation in Fig. 4(c). The calculated spectral envelope has been dramatically reduced and is in better agreement with the experimental spectrum than with the

simulation using Cartesian coordinates. The normal mode simulations of $CHCl_2^-$, $CHBr_2^-$, $CDBr_2^-$, $CHI_2^-$, and $CDI_2^-$ using internal coordinates display a similar quality of agreement with the experimental spectra (Fig. S2(a), Fig. S3, and Fig. S4).[47] Using the estimated EAs from the calculations, the band maxima of these simulations are in improved agreement with the experimental bands. However, the simulations using internal coordinates still have broader envelopes than what we observe experimentally, and the partially resolved vibrational structure in the experiments is not reproduced in the simulations.

The normal mode analysis of molecular vibrations is valid for small displacements from the equilibrium geometry. For infinitesimal displacements, the normal coordinate vectors are identical whether represented in terms of internal coordinates (bond stretches and angles) or in terms of Cartesian atom-displacement coordinates, i.e., the displacement vectors are tangent at the equilibrium geometry. For a large change along a normal coordinate, the curvilinear internal coordinates system and the rectilinear Cartesian displacements lead to different values of the displacement [element **K″** for the normal mode, Eq. (2)] for the same molecular geometry change. As the vibrational potential energy surface is more naturally described in terms of internal coordinates, they tend to provide more physically accurate normal coordinate displacements. The curvilinear internal coordinates provide a much better first-order approximation to the natural nuclear motion. In particular for these systems, the Franck–Condon intensities using internal coordinates exhibit no significant contribution from the CH stretch mode.

The extended vibrational progression in disagreement with the experimental spectral envelope results from the method used to simulate the spectra, and not from errors in the electronic structure calculations. This fact is evidenced by the accuracy of the VDE calculation using B3LYP/6–311++G(d,p), illustrated in Fig. 3. Earlier DFT calculations by Li *et al.*[30] demonstrate similar agreement with our experimental results and with previous EA measurements of $CHCl_2$ and $CHBr_2$.[29] As the VDE can be accurately calculated using DFT methods, it is clear that the harmonic normal mode simulation—and not the electronic structure calculations—is at fault for the failure to reproduce the spectral envelopes of the dihalomethyl anions. Though the agreement between simulation and experiment is too poor to use to determine the EA, the calculated VDEs can be employed without simulation to obtain an estimate of the EA. Using Eq. (8), we obtain EA estimates that are consistent with previous measurements (Table III).

Although the qualitative agreement is reasonable, the simulation using internal coordinates is still not completely adequate in explaining the experimental bandwidth or vibrational structure. The failure of this method to reproduce the experimental photoelectron spectra accurately is a result of several factors. The large difference in equilibrium geometries and bonding between the anion and neutral cause the normal modes of the neutral to be characteristically different than those of the anion. Thus, when the normal modes of the neutral are expressed in terms of harmonic normal mode vibrations of the anion, orthogonality of the neutral

normal modes is lost, resulting in mode mixing. Additionally, the neutral out-of-plane bending mode is clearly anharmonic, and representing this vibration as a harmonic oscillator is another source of discrepancy with experiment. Furthermore, because we are sampling high vibrational levels of the neutral molecule for which there are multiple active vibrational modes of similar frequency, there is considerable possibility for coupling between the vibrational modes expected to be important. The normal mode approach to simulating the photoelectron spectra of the dihalomethyl anions has proven insufficient to elucidate the spectra, and we next take a multidimensional coupled-mode approach to computing the photoelectron spectra.

## D. Multidimensional approach for $CHCl_2$ and $CDCl_2$

The $CDCl_2^-$ photoelectron spectrum calculated using the multidimensional coupled-mode approach outlined in Sec. III D is shown in Fig. 4(d). The calculated spectrum shown in the figure displays much improved agreement with experiment. Similar improvement over the normal mode approach in internal coordinates is shown for $CHCl_2^-$ [Fig. S2 (b)].[47] Reduced dimensional analysis shows that 98% of the overlap between the $CHCl_2^-$ ground vibrational state in the CH stretching coordinate ($v''_{CH} = 0$) occurs with $v'_{CH} = 0$ in $CHCl_2$. Thus, the CH (CD) stretch contributes negligible intensity above the 0–0 origin transition. Significant reduction in the width of the spectral envelope compared to the two harmonic treatments discussed above results from a combination of the inclusion of anharmonicity in each of the three modes that are considered as well as allowing for mode-mode coupling among the two bending degrees of freedom.

The extent of the coupling between the two bending vibrations $\tau_{ClCDCl'}$ and $\theta_s$ is illustrated in Fig. 5, which shows the development of the two-dimensional $CDCl_2$ wavefunction (color contours) with increasing energy. Wavefunctions are plotted as a function of the out-of-plane distortions ($\tau_{ClCDCl'}$) and the symmetric combination of the two DCCl bends ($\theta_s = \sqrt{2}\theta_{DCCl}$). These two internal coordinates, $\tau_{ClCDCl'}$ and $\theta_s$, were chosen because they are a natural pair of vibrations that are coupled to each other but are reasonably decoupled from other modes, as illustrated in Fig. 2. The wavefunction for the lowest energy state of $CDCl_2$, shown in Fig. 5(a), displays the greatest probability between $\tau_{ClCDCl'} = 150°$ and $210°$ with a maximum at $180°$, indicating that in its ground vibrational state, the neutral species displays large amplitude displacements from the equilibrium geometry through the planar structure. The next higher energy state in this two-dimensional model is depicted in Fig. 5(b). Figures 5(a) and 5(b) show the lack of Franck–Condon overlap between the anion wavefunction (gray contours) and low vibrational levels of the neutral, resulting in our inability to experimentally observe the origin peak. From these plots, it is evident that even at low vibrational levels of the neutral, these two modes are strongly coupled, as activation of the $\tau_{ClCDCl'}$ bend is accompanied by a comparable change in $\theta_s$.

Coupling between $\tau_{ClCDCl'}$ and $\theta_s$ becomes even more pronounced at higher vibrational levels of the neutral with
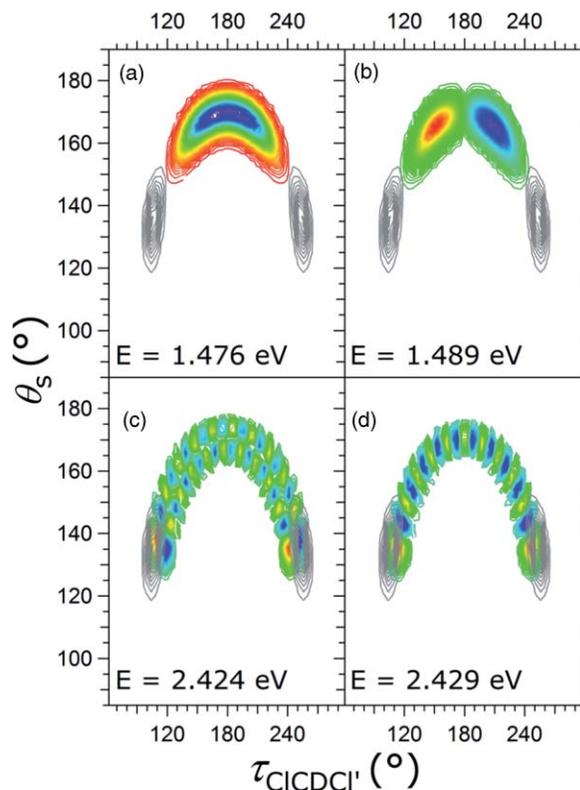
FIG. 5. Plots of the two-dimensional wavefunctions of CDCl$_2$ and CDCl$_2{}^-$. The wavefunction of the ground vibrational state of CDCl$_2{}^-$ is shown with gray contours, and the CDCl$_2$ wavefunctions are shown in color contours. The energy of the CDCl$_2$ wavefunction relative to the zero-point energy of the anion is given in each panel. There is negligible Franck–Condon overlap of the ground-state anion wavefunction with the ground-state neutral wavefunction (a) and with the first excited vibrational level of the neutral (b). The best overlap (c) is calculated to occur 2.424 eV above the zero-point energy of CHCl$_2{}^-$. (d) The next higher vibrational level of CDCl$_2$, in which one quantum of excitation in $\theta_s$ is exchanged for an additional quantum of excitation in $\tau_{\text{ClCDCl}'}$, lies only 5 meV higher in energy. This resonance leads to the highly structured CDCl$_2$ spectrum.



FIG. 6. (a) The 150 K experimental photoelectron spectrum of CDCl$_2{}^-$ is shown in black, and the multidimensional coupled-mode simulation is overlaid in blue. Dark blue sticks correspond to the most intense transitions in the two-dimensional coupled bend coordinate. Coincidental resonances of these transitions account for the highly structured spectrum of CDCl$_2{}^-$. (b) The inset shows a close-up of the agreement between the experimental and calculated spectra near the vertical detachment energy.

energies near the VDE, where the Franck–Condon overlap with the ground vibrational wavefunction of the anion is greatest. Figure 5(c) shows the two-dimensional CDCl$_2$ wavefunction that has the largest Franck–Condon overlap with the ground vibrational wavefunction of CDCl$_2{}^-$; this transition contributes the most intensity to the calculated photoelectron spectrum. The two-dimensional wavefunction of the vibrational level shown in Fig. 5(c) displays the greatest probability at the turning points, which is physically manifested as a large amplitude bending motion in $\tau_{\text{ClCDCl}'}$. Also notice that the shape of the wavefunction mimics the shape of the curve in Fig. 2(a); i.e., the two-dimensional wavefunction follows the minimum energy curve in the $\theta_{\text{DCCl}}$ and $\tau_{\text{ClCDCl}'}$ coordinates. In both Figs. 5(c) and 2(a), we see that the $\tau_{\text{ClCDCl}'}$ bend is accompanied by a large change in $\theta_s$, again indicating significant coupling between these vibrational modes. Coupling of low frequency vibrations along with the highly anharmonic nature of the low frequency bend provides two sources for the breakdown of the normal mode approximation for the dihalomethyl radicals, since we can no longer treat the vibrations as products of harmonic oscillator wavefunctions. While alternative choices of the bend coordinates could reduce the
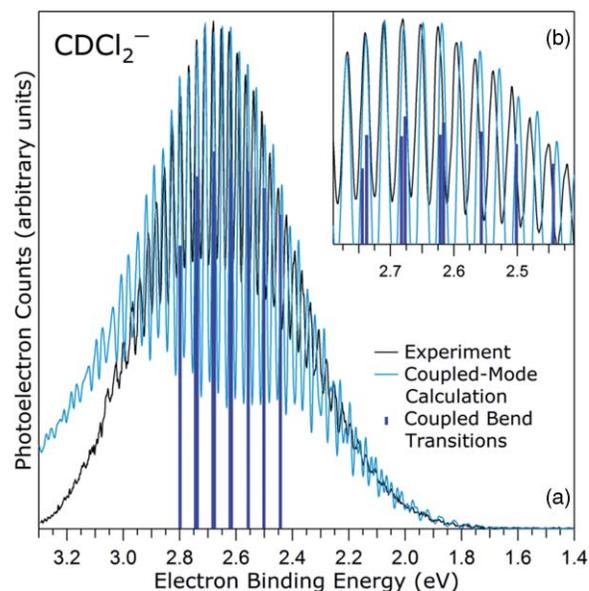
coupling, these choices will also affect the separability of the ground state wavefunction on the anionic potential surface.

The structure of the spectra and the counterintuitive consequences of isotopic substitution arise from near degeneracies of the frequencies high in the potential well, where the Franck–Condon overlap is the greatest. This resonance is illustrated in panels (c) and (d) of Fig. 5. The vibrational state with the most intensity in the CDCl$_2{}^-$ photoelectron spectrum [Fig. 5(c)] corresponds to one quantum of excitation in $\theta_s$ and 19 quanta of excitation in the out-of-plane distortion $\tau_{\text{ClCDCl}'}$. The next highest energy state within this two-dimensional model, shown in Fig. 5(d), also contributes significantly to the spectrum (93% of the intensity of the most intense transition); this state corresponds to zero quanta of excitation in $\theta_s$ and 20 quanta of excitation in $\tau_{\text{ClCDCl}'}$. These two levels are separated by ∼5 meV; within our instrument resolution, these two transitions appear as a single peak in the photoelectron spectrum. This is true of the coupled-bend vibrational levels of CDCl$_2$ near the VDE: "exchanging" one quantum of excitation in $\theta_s$ for an additional quantum of excitation in $\tau_{\text{ClCDCl}'}$ results in peaks separated by only 5 meV, and thus they appear as a single peak. The manifestation of this accidental degeneracy is displayed in Fig. 6; blue sticks correspond to the 10 most intense $\theta_s$ and $\tau_{\text{ClCDCl}'}$ transitions. The near-resonance results in a highly structured CDCl$_2{}^-$ photoelectron spectrum. The bend and out-of-plane distortions account for half of the observed peaks; the remaining peaks result from excitation of the ClCCl symmetric stretch.

In the case of CHCl$_2$, such a resonance of the $\theta_s$ and $\tau_{\text{ClCHCl}'}$ transitions does not occur, and the vibrational structure is significantly more congested. While exchanging one
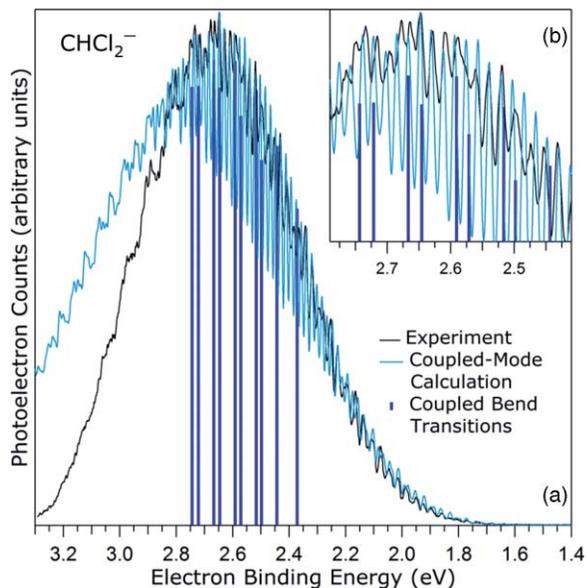
FIG. 7. (a) The 150 K experimental photoelectron spectrum of $CHCl_2^-$ is shown in black, and the multidimensional coupled-mode calculated spectrum is overlaid in blue. Dark blue sticks correspond to the most intense vibronic transitions in the two-dimensional coupled bend coordinate. (b) The inset shows a close-up of the agreement between the experimental and calculated spectra near the vertical detachment energy.

quantum of excitation in $\theta_s$ for an additional quantum of excitation in $\tau_{ClCDCl'}$ results in peaks separated by only 5 meV in $CDCl_2$, such a trade results in peaks separated by $\sim$20 meV, as shown in Fig. S5.[47] Figure 7 shows the effect of this lack of resonance on the spectrum of $CHCl_2^-$. Here again, the 10 most intense coupled bend transitions are shown in blue sticks. The 20 meV spacing between consecutive $\theta_s$ and $\tau_{ClCHCl'}$ vibrational transitions near the VDE is experimentally resolvable; when added to the ClCCl symmetric stretch contribution—which is largely unaffected by deuteration—we observe a congested photoelectron spectrum. Thus, the counterintuitive effect of deuteration on the $CHCl_2^-$ and $CDCl_2^-$ spectra is a result of the near-resonance, or lack thereof, between the $\theta_s$ and $\tau_{ClCHCl'}$ coupled-bend vibrational transitions at the very high vibrational levels accessed.

The multidimensional coupled-mode analysis qualitatively reproduces the photoelectron spectra of $CHCl_2^-$ and $CDCl_2^-$ and yields a substantial improvement over normal-mode analysis for these molecules in terms of both the extent of the spectral envelope and peak spacing. Table III compares the average peak spacing near the VDE in the experimental spectra to peak spacing in the calculated spectra using both the harmonic normal mode and the anharmonic coupled-mode analyses. While the agreement in the width of the spectral envelope and in the peak spacing is much improved in the multidimensional approach, it is still not completely sufficient to yield reliable estimates of EAs or vibrational frequencies. Even after tackling the problem using the most sophisticated and computationally expensive multidimensional approach, our best estimates of the EAs are obtained through direct application of the calculated VDEs, via Eq. (8), without the aid of any simulations.

## V. CONCLUSIONS

The pyramidal dihalomethyl anions become nearly planar upon photodetachment, resulting in photoelectron spectra that display extended vibrational progressions with no intensity at the origin transition. The absence of experimentally observable origins in the spectra and the inability to accurately reproduce the spectral envelopes preclude the direct determination of EAs or vibrational frequencies of the dihalomethyl anions in this study. While normal mode analysis accurately simulates the spectra of molecules that experience small displacements of equilibrium nuclear configurations upon photodetachment, false activity of the CH stretch is predicted in the dihalomethyl radicals when a Cartesian displacement coordinate system is employed. Use of internal coordinates for the normal mode analysis eliminates that problem, but the Franck–Condon simulations using independent harmonic oscillators are still inadequate. The harmonic Franck–Condon simulation using internal coordinates yields a spectral envelope that is too broad. The calculated VDE is in agreement with the measured VDE. Therefore, the inability to reproduce the shape of the vibrational progression must be an artifact of the method used to compute the FCFs.

In order to simulate the spectra of the dihalomethyl radicals with more accuracy, we take a multidimensional anharmonic coupled-mode approach. The coupling of the multiple active low-frequency bending vibrations is the source of the breakdown of the normal mode approximation for the dihalomethyl radicals; consequently, we cannot treat the vibrations as separable, nor compute FCFs as the product of harmonic oscillators. Instead, using $(2 + 1)$-dimensional analysis, we calculate negligible contribution from the CH stretch above the 0–0 transition and find that coupled $\tau_{ClCHCl'}$ and $\theta_s$ bends plus the ClCCl symmetric stretch fully account for the observed structure in the $CHCl_2^-$ and $CDCl_2^-$ spectra.

Unfortunately, there is no reliable, general approach to analyzing the Franck–Condon bands of transitions involving large geometry changes, such as those of the dihalomethyl anions. Normal mode analysis in an internal coordinate representation yields much better results than using rectilinear Cartesian displacement coordinates, but it requires Wilson's GF method to compute Duschinsky translation vectors and rotation matrices and still fails to adequately reproduce the width of the spectral envelope for these systems. Multidimensional anharmonic coupled-mode analysis achieves reasonable agreement with the observed spectra of the dihalomethyl anions; however, these calculations are computationally expensive, precluding determination of molecular parameters by direct fitting to the observed spectra and are also specific to each molecule studied. In fact, the best experimental EA estimates of the dihalomethyl radicals are obtained by directly employing the difference in energy between the calculated VDE and calculated EA. With effort, we can understand the spectra of the dihalomethyl anions, but we are unable to obtain the quantitative information that can be determined from the photoelectron spectra of more rigid molecules.

This leaves us with the question of how one can anticipate the breakdown of harmonic treatments. In the absence of prior knowledge of the EAs, there are few clues in the measured

photoelectron spectra of the dihalomethyl anions that would lead one to anticipate the need to perform anharmonic calculations. A full discussion of this issue is beyond the scope of the present study, although this work sheds light on several of the factors that could be used to anticipate difficulties with harmonic treatments. First, there is a large structural change between the anion and the neutral, as displayed by the large change in $\tau_{ClCHCl'}$ upon photodetachment (Table II). This leads to a change in the definition of the normal modes that are used to expand the wavefunctions for the anion and for the neutral. The second important factor is the low frequency and large anharmonicity in the vibrational mode associated with displacements in $\tau_{ClCHCl'}$. This leads to the sampling of very highly excited bend states on the neutral surface upon electron detachment. In the dihalomethyl radicals, the low frequency and large anharmonicity of this mode are anticipated by barriers to planarity that are lower than the harmonic zero-point energy of this mode. The high level of vibrational excitation of these anharmonic modes makes such systems challenging for approaches that are based on harmonic treatments.

## ACKNOWLEDGMENTS

[1] E. S. Whitney, T. Haeber, M. D. Schuder, A. C. Blair, and D. J. Nesbitt, J. Chem. Phys. **125**, 054303 (2006).

[2] M. Schwartz, L. R. Peebles, R. J. Berry, and P. Marshall, J. Chem. Phys. **118**, 557 (2003).

[3] M. J. Molina, L. T. Molina, and C. E. Kolb, Annu. Rev. Phys. Chem. **47**, 327 (1996).

[4] B. J. Finlayson-Pitts, *Chemistry of the Upper and Lower Atmosphere: Theory, Experiments, and Applications* (Academic, New York, 1999).

[5] J. S. Francisco and M. M. Maricq, in *Advances in Photochemistry* (Wiley, New York, 1995), Vol. 20, pp. 79.

[6] L. J. Carpenter, Chem. Rev. **103**, 4953 (2003).

[7] M. McFarland and J. Kaye, Photochem. Photobiol. **55**, 911 (1992).

[8] S. I. Stoliarov, A. Bencsura, E. Shafir, V. D. Knyazev, and I. R. Slagle, J. Phys. Chem. A **105**, 76 (2001).

[9] H. E. Simmons and R. D. Smith, J. Am. Chem. Soc. **81**, 4256 (1959).

[10] D. C. Blomstrom, K. Herbig, and H. E. Simmons, J. Org. Chem. **30**, 959 (1965).

[11] N. J. Pienta and P. J. Kropp, J. Am. Chem. Soc. **100**, 655 (1978).

[12] P. J. Kropp, N. J. Pienta, J. A. Sawyer, and R. P. Polniaszek, Tetrahedron **37**, 3236 (1981).

[13] P. J. Kropp, Acc. Chem. Res. **17**, 131 (1984).

[14] E. C. Friedrich, J. M. Domek, and R. Y. Pong, J. Org. Chem. **50**, 4640 (1985).

[15] E. C. Friedrich, S. E. Lunetta, and E. J. Lewis, J. Org. Chem. **54**, 2388 (1989).

[16] S. Durandetti, S. Sibille, and J. Perichon, J. Org. Chem. **56**, 3255 (1991).

[17] J. M. Concellon, P. L. Bernad, and J. A. Perez-Andres, Tetrahedron Lett. **39**, 1409 (1998).

[18] T. G. Carver and L. Andrews, J. Chem. Phys. **50**, 4235 (1969).

[19] T. G. Carver and L. Andrews, J. Chem. Phys. **50**, 4223 (1969).

[20] M. E. Jacox and D. E. Milligan, J. Chem. Phys. **54**, 3935 (1971).

[21] B. S. Ault and L. Andrews, J. Chem. Phys. **63**, 1411 (1975).

[22] M. E. Jacox, Chem. Phys. **12**, 51 (1976).

[23] L. Andrews, F. T. Prochaska, and B. S. Ault, J. Am. Chem. Soc. **101**, 9 (1979).

[24] L. Andrews and F. T. Prochaska, J. Am. Chem. Soc. **101**, 1190 (1979).

[25] T. D. Fridgen, X. K. K. Zhang, J. M. Parnis, and R. E. March, J. Phys. Chem. A **104**, 3487 (2000).

[26] A. Richter, H. Meyer, T. Kausche, T. Muller, W. Sporleder, and A. Schweig, Chem. Phys. **214**, 321 (1997).

[27] D. K. Bohme, L. B. Young, and E. Leeruff, J. Am. Chem. Soc. **94**, 5153 (1972).

[28] J. L. Holmes and F. P. Lossing, J. Am. Chem. Soc. **110**, 7343 (1988).

[29] M. Born, S. Ingemann, and N. M. M. Nibbering, Int. J. Mass Spectrom. **194**, 103 (2000).

[30] Q. S. Li, J. F. Zhao, Y. M. Xie, and H. F. Schaefer, Mol. Phys. **100**, 3615 (2002).

[31] K. M. Ervin and W. C. Lineberger, in *Advances in Gas Phase Ion Chemistry*, edited by N. G. Adams and L. M. Babcock (JAI, Greenwich, 1992), Vol. 1, pp. 121.

[32] D. G. Leopold, K. K. Murray, A. E. S. Miller, and W. C. Lineberger, J. Chem. Phys. **83**, 4849 (1985).

[33] K. M. Ervin, J. Ho, and W. C. Lineberger, J. Chem. Phys. **91**, 5974 (1989).

[34] S. W. Wren, K. M. Vogelhuber, K. M. Ervin, and W. C. Lineberger, Phys. Chem. Chem. Phys. **11**, 4745 (2009).

[35] C. S. Feigerle, Ph.D. dissertation, University of Colorado, 1983.

[36] D. M. Neumark, K. R. Lykke, T. Andersen, and W. C. Lineberger, Phys. Rev. A **32**, 1890 (1985).

[37] C. E. Moore, Circular of the National Bureau of Standards 467, 1958.

[38] J. Cooper and R. N. Zare, J. Chem. Phys. **48**, 942 (1968).

[39] M. J. Frisch, G. W. Trucks, H. B. Schlegel *et al.*, GAUSSIAN 03, Revision B.01, Gaussian, Inc., Wallingford, CT, 2004.

[40] A. D. Becke, J. Chem. Phys. **98**, 5648 (1993).

[41] C. T. Lee, W. T. Yang, and R. G. Parr, Phys. Rev. B **37**, 785 (1988).

[42] A. D. McLean and G. S. Chandler, J. Chem. Phys. **72**, 5639 (1980).

[43] R. Krishnan, J. S. Binkley, R. Seeger, and J. A. Pople, J. Chem. Phys. **72**, 650 (1980).

[44] H. Stoll, B. Metz, and M. Dolg, J. Comput. Chem. **23**, 767 (2002).

[45] M. A. Thompson, J. P. Martin, J. P. Darr, W. C. Lineberger, and R. Parson, J. Chem. Phys. **129**, 224304 (2008).

[46] M. A. Thompson, Ph.D. dissertation, University of Colorado, 2007.

[47] See supplementary material at http://dx.doi.org/10.1063/1.3585606 for a table of the calculated frequencies (TABLE S1) and equilibrium structures (TABLE S2) of $CHBr_2$ and $CDBr_2$; for a table of the calculated frequencies (TABLE S3) and equilibrium structures (TABLE S4) of $CHI_2$ and $CDI_2$; for two-dimensional cuts through the $CHCl_2^-$ and $CHCl_2$ potential energy surfaces (Fig. S1); for a comparison of the $CHCl_2^-$ spectrum to its normal mode simulation in internal coordinates and to its calculated spectrum using multidimensional coupled-mode analysis (Fig. S2); for a comparison of the $CHBr_2^-$ and $CDBr_2^-$ (Fig. S3) and the $CHI_2^-$ and $CDI_2^-$ (Fig. S4) spectra to their simulations using the Sharp-Rosenstock-Chen method in internal coordinates; and for plots of the $CHCl_2$ and $CHCl_2^-$ wavefunctions (Fig. S5).

[48] K. M. Ervin, J. Ho, and W. C. Lineberger, J. Phys. Chem. **92**, 5405 (1988).

[49] F. Duschinsky, Acta Physicochim. URSS **7**, 551 (1937).

[50] K. M. Ervin, PESCAL, Fortran program, University of Nevada, Reno (2010).

[51] *Unimolecular and Bimolecular Ion-Molecule Reaction Dynamics*, edited by P. Chen (Wiley, Chichester, 1994).

[52] K. M. Ervin, T. M. Ramond, G. E. Davico, R. L. Schwartz, S. M. Casey, and W. C. Lineberger, J. Phys. Chem. A **105**, 10822 (2001).

[53] T. E. Sharp and H. M. Rosenstock, J. Chem. Phys. **41**, 3453 (1964).

[54] W. D. Gwinn, J. Chem. Phys. **55**, 477 (1971).

[55] E. B. Wilson, J. C. Decius, and P. C. Cross, *Molecular Vibrations* (Dover, New York, 1980).

[56] J. H. Frederick and C. Woywod, J. Chem. Phys. **111**, 7255 (1999).

[57] J. R. Reimers, J. Chem. Phys. **115**, 9103 (2001).

[58] R. Borrelli and A. Peluso, J. Chem. Phys. **125**, 194308 (2006).

[59] D. T. Colbert and W. H. Miller, J. Chem. Phys. **96**, 1982 (1992).

[60] D. Luckhaus, J. Chem. Phys. **113**, 1329 (2000).

[61] G. H. Gardeinier, M. A. Johnson, and A. B. McCoy, J. Phys. Chem. A **113**, 4772 (2009).

[62] J. R. Reimers and R. O. Watts, Mol. Phys. **52**, 357 (1984).

[63] J. R. Reimers, K. R. Wilson, E. J. Heller, and S. R. Langhoff, J. Chem. Phys. **82**, 5064 (1985).

[64] K. M. Vogelhuber, S. W. Wren, L. Sheps, and W. C. Lineberger, J. Chem. Phys. **134**, 064302 (2011).

[65] H. Kikuchi, M. Kubo, N. Watanabe, and H. Suzuki, J. Chem. Phys. **119**, 729 (2003).

[66] R. Borrelli and A. Peluso, J. Chem. Phys. **128**, 044303 (2008).

[67] G. R. Long and J. W. Hudgens, J. Phys. Chem. **91**, 5870 (1987).